International Journal of Micro Air Vehicles

Article

International Journal of Micro Air Vehicles
2018, Vol. 10(4) 370–385

DOI: 10.1177/1756829318809706
journals.sagepub.com/home/mav
SAGE

Performance analysis of vertically offset overlapped propulsion system based quadrotor in an aerial mapping mission

Ganeshram Nandakumar[1], Rohan Saphal[1], Ashish Joishy[2] and Asokan Thondiyath[1]

Abstract

In this paper, the authors present the performance analysis of a Vertically Offset Overlapped Propulsion System (VOOPS)-based quadrotor in an aerial mapping mission. The dynamic model of the VOOPS quadrotor with the effect of overlapping propellers and the profile drag has been derived and simulated. A path-tracking mission is taken as an example for aerial survey. The controller used for this task is presented, followed by the response study of the attitude and the position controller with standard test inputs. A graphical interface has been built to select the area to be mapped by defining a polygon around it, and waypoints for lawn-mower type survey grid were generated based on the direction of wind. The path-tracking algorithm is presented along with course correction and simulations were performed with both conventional and VOOPS quadrotor. An experimental vehicle based on the proposed VOOPS concept has been built, tested on the same path, and the results are discussed. The results show that the VOOPS quadrotor is capable of performing the aerial mapping mission with quick response and good accuracy.

Keywords

Overlapped propellers, aerial mapping, unmanned aerial vehicle, multirotor, quadrotor, path tracking, mission planner

Received 28 June 2017; accepted 11 July 2018

Introduction

Aerial robot systems are primarily being developed for military applications like surveillance, reconnaissance, and mapping. Geomatics (the branch of science that deals with the collection, analysis, and interpretation of data relating to the earth's surface) is another area where aerial robots are finding wide applications. This is due to the price drop of unmanned aerial vehicle (UAV) components and development of advanced hardware.[1,2] The low-cost navigational systems and the current development in UAV platforms along with light-weight, high-resolution cameras have enabled surveying sector to use such technologies.[3] It is definitely a replacement to the classical ground-based methods which are time consuming. Satellite imagery has an advantage of large area coverage but it lacks resolution. Although conventional remote sensing using manned aircraft has great advantages like better resolution, large coverage and capability to carry high-resolution cameras, UAV platforms can provide better resolution and make the mapping process economical and easy due to the advantage of being able to fly closer to the ground. They are a very important requirement when a small area has to be surveyed with centimetre level accuracy, where the manned aircraft or satellite imagery cannot attain the level of resolution that a UAV-based system can achieve. The resolution of the maps generated by aerial mapping depends on the resolution of the camera equipment used to shoot the images and the height at which the camera shots were taken. If the imaging is done closer

[1]Department of Engineering Design, Indian Institute of Technology Madras (IITM), Chennai, India
[2]Department of Mechanical Engineering, National Institute of Technology, Surathkal, India

Corresponding author:
Asokan Thondiyath, Department of Engineering Design, Indian Institute of Technology Madras (IITM), Chennai, India.
Email: asok@iitm.ac.in

to ground the shutter speed and light gathering capability of the imaging equipment becomes important. This is to have enough light and avoid motion blur. This demands for a slow and low-flying UAV where fixed-wing-type UAV's are not an option. Hence one has to look at a VTOL (Vertical Take Off and Landing)-based UAV. Multirotor is the best option as they are more reliable than single rotor UAV's. The quadrotor UAV's for a given size suffers endurance and payload limitations and even a small improvement will help in carrying better camera equipment and cover larger area. The design of compact VTOL UAV with an improved endurance and payload capability is challenging as they are conflicting design requirements. Some research work to improve endurance such as, downward mounted propellers configuration,[4,5] decoupling of the stabilization and the lifting tasks,[6,7] discarding consumed batteries,[8] etc., were reported, but there was not much focus on the design modifications. Designing a quadrotor with high payload capacity and endurance for a given footprint is onerous and demands novel design approach. A novel concept of overlapping propellers at different planes for a quadrotor system was proposed by the authors in 2015, named as Vertically Offset Overlapping Propulsion System (VOOPS),[9] inspired by the tandem rotors configuration found in Piasecki HRP Rescuer.[10] The main objective here was to accommodate larger propellers by making design changes in the conventional quadrotor-based VTOL system. The propellers are allowed to overlap by placing them at different planes separated by a distance in such a way that they do not interfere with each other. The utility of VOOPS for aerial mapping applications is analysed in this paper. The design details of VOOPS and its mathematical modelling are presented in the beginning followed by issues related to aerial mapping using quadrotors, and the design of controllers for the mapping mission. Sections on simulation studies and aerial mapping present the simulation and experimental results of aerial mapping using VOOPS quadrotor and the advantages VOOPS offer.

VOOPS concept

As the name suggests, Vertically Offset Overlapping Propulsion System is a design concept where the propellers are vertically offset to enable overlap as shown in Figure 1. This design concept when implemented improves endurance and payload capacity without affecting the footprint, which was not feasible using a conventional quadrotor design.[11]

VOOPS is designed as a bi-layered frame, with the layers offset by a distance 'O_z' vertically as shown in Figure 1. Each layer accommodates two rotors, U_1 and U_2 on top layer and L_1 and L_2 in bottom layer. The crucial factors in the VOOPS configuration are the overlap and offset between the blades. The following sections explain the mathematic model, thrust loss due to overlap and power consumption of the VOOPS design.

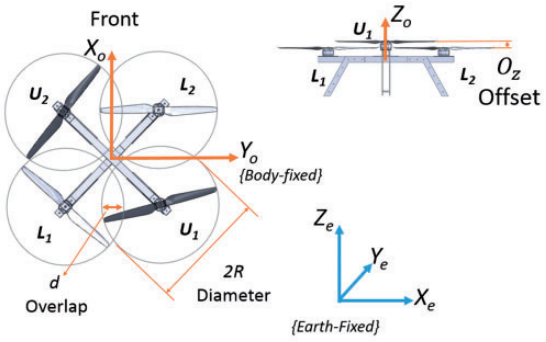

Figure 1. VOOPS configuration.

Mathematical model

Dynamic model

The dynamic model of VOOPS quadrotor can be derived using Lagrangian/Newtonian mechanics as given below. The rotational dynamics can be represented as

$$\begin{aligned}
\ddot{\phi} &= \dot{\theta}\dot{\psi}\left(\frac{I_{Y_o}-I_{Z_o}}{I_{X_o}}\right) - \left(\frac{J_r}{I_{X_o}}\right)\dot{\theta}\Omega \\
&\quad + \left(\frac{1}{I_{X_o}}\right)M_\phi + \left(\frac{l}{I_{X_o}}\right)(T_{lossL_2} - T_{lossL_1}) \\
\ddot{\theta} &= \dot{\phi}\dot{\psi}\left(\frac{I_{Z_o}-I_{X_o}}{I_{Y_o}}\right) + \left(\frac{J_r}{I_{Y_o}}\right)\dot{\phi}\Omega \\
&\quad + \left(\frac{1}{I_{Y_o}}\right)M_\theta + \left(\frac{l}{I_{Y_o}}\right)(T_{lossL_2} - T_{lossL_1}) \\
\ddot{\psi} &= \dot{\phi}\dot{\theta}\left(\frac{I_{X_o}-I_{Y_o}}{I_{Z_o}}\right) + \left(\frac{1}{I_{Z_o}}\right)M_\psi
\end{aligned} \tag{1}$$

where ϕ, θ and ψ are the roll, pitch and yaw angles respectively, and J_r is the combined rotor and propeller inertia. Ω is used to calculate the propeller induced gyroscopic effect[12] and is given by $\Omega = \Omega_{L_1} + \Omega_{L_2} - \Omega_{U_2} - \Omega_{U_1}$ where, $\Omega_{U_i}, \Omega_{L_i}$ are the angular velocities of the upper and lower rotors. M_ϕ, M_θ and M_ψ are the external moments acting on the quadrotor and I_{X_o}, I_{Y_0} and I_{Z_o} are the moment of inertia of the quadrotor system about X_o, Y_o and Z_o axis respectively. l is half the distance between the adjacent rotors. The equations contain the term T_{lossL_i}, which includes the losses incurred due to the overlapping propellers.

The translational dynamics can be represented using equation (2). Here, T is the collective force acting in the

Z_o direction.

$$\begin{bmatrix} \ddot{Z}_e \\ \ddot{X}_e \\ \ddot{Y}_e \end{bmatrix} = \left(\frac{1}{m}\right) \begin{bmatrix} -g + (\cos\phi\cos\theta)(T + T_{lossL_1} + T_{lossL_2} + F_x) \\ (\cos\phi\sin\theta\cos\psi + \sin\phi\sin\psi)(T + T_{lossL_1} + T_{lossL_2} + F_y) \\ (\cos\phi\sin\theta\sin\psi - \sin\phi\cos\psi)(T + T_{lossL_1} + T_{lossL_2} + F_z) \end{bmatrix} \quad (2)$$

where $\ddot{X}_e$, $\ddot{Y}_e$ and $\ddot{Z}_e$ are the accelerations with respect to the earth-fixed frame, and F_i is the drag force acting on the quadrotor on the ith axis, due to the relative velocity of wind, where $i = X_o, Y_o, Z_o$ and is derived in the following section. The force and moment[13] generated due to the propeller rotation can be obtained as

$$\begin{aligned} T &= b\left(\Omega_{L_1}^2 + \Omega_{L_2}^2 + \Omega_{U_2}^2 + \Omega_{U_1}^2\right) \\ M_\phi &= lb\left(\Omega_{L_1}^2 - \Omega_{L_2}^2 + \Omega_{U_2}^2 - \Omega_{U_1}^2\right) \\ M_\theta &= lb\left(\Omega_{L_1}^2 - \Omega_{L_2}^2 - \Omega_{U_2}^2 + \Omega_{U_1}^2\right) \\ M_\psi &= k\left(\Omega_{L_1}^2 + \Omega_{L_2}^2 - \Omega_{U_2}^2 - \Omega_{U_1}^2\right) \end{aligned} \quad (3)$$

where $b = \rho A R^2 C_t$ and $k = \rho A R^3 C_q$. ρ is the density of air, A is the area of the propeller disk, R is the radius of the propeller, and C_q and C_t are the coefficient of drag torque and thrust respectively. The thrust loss due to overlapping of propellers can be estimated using the aerodynamic analysis of the propellers, as explained in the following sections.

Aerodynamic model

In this section, the aerodynamics of the propeller in the overlapped region is discussed, followed by the model of profile drag experienced by the quadrotor.

Model of an overlapping propeller. Based on the Blade Element Theory (BET), the forces acting on each elemental section are integrated along the span to find the net aerodynamic forces.[14]

Consider one blade of the rotor at an angular position, shown as LN in Figure 2, LM is the region close to hub not affected by the inflow, MN is the region affected by the inflow from the upper propeller. The points M and N will vary depending on the overlap percentage and the position of the propeller, and the distance LM is defined as X_1 and LN as X_2. Thrust produced in the overlapped region can be found by integrating thrust produced by the blade sections MN (X_1 *to* X_2) in the overlapped region. Overlapped region can be defined with respect to the angular position of the propeller ψ_i, where $i = 1, 2$ which represents the start and end of overlapped region. T_{lossL_i} is the loss incurred in the overlapped region (shown as dark grey in the Figure 2) which can be calculated from blade geometry, amount of overlap and offset as given by the equation (4).

$$T_{lossL_i} = \Omega_{L_i}(\Omega_{U_1} + \Omega_{U_2})\frac{\rho A R^2}{2\pi}\int_{\psi_1}^{\psi_2}\int_{X_1}^{X_2}\sigma_l C_L \lambda_u r \mathrm{d}r\mathrm{d}\psi \quad (4)$$

where σ_l, the solidity ratio, can be given as $\sigma_l = nc(r)/\pi R.r$ is the distance from the hub, n is the number of blades in a propeller, C_L is the lift curve slope for the propeller, c is the chord length of the propeller at r and λ_u is the inflow ratio of the upper propeller. Using equation (4), thrust loss in the overlapped region of a lower propeller, for various speeds of the upper and lower propellers can be computed. A visualisation of the thrust loss is shown in Figure 3 for a propeller of 15 inch throughout the operating range of rotor speeds.

It is seen that for a non-zero angular velocity of the lower propeller the loss in thrust increases as either of the upper propeller's angular velocity increases. The maximum loss[15] is around 25% (~4.41 N) at peak angular velocity (6600 r/min) of all the three rotors and at a normal operating angular velocity (3300 r/min), the loss is seen to be less than 5% (~0.98 N).

Profile drag. It is straight forward to estimate the drag force, **f** by knowing the drag coefficient of the vehicle, C_D and the area exposed. The area, **a** exposed to the

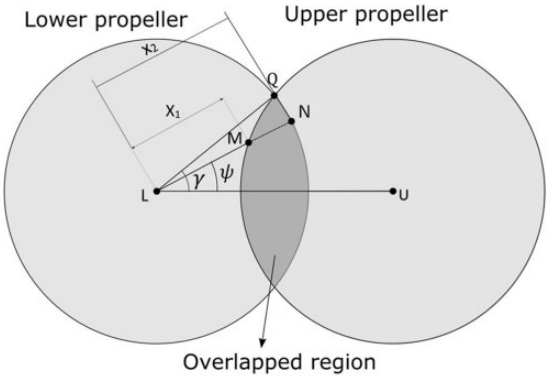

Figure 2. Schematic representation of blade overlap.

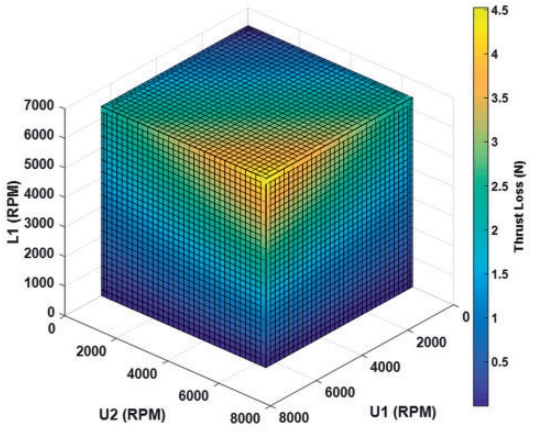

Figure 3. Thrust loss in lower propeller.

wind is a function of the roll and pitch of the quadrotor and is computed using equation (5).

$$\mathbf{a} = 4S_p R^2 \pi \begin{bmatrix} \sin\theta \cos\phi \\ \sin\phi \cos\theta \\ \cos\phi \cos\theta \end{bmatrix} \tag{5}$$

where S_p is the coefficient that expresses the semi-permeable nature of the rotating propeller and it varies from 0 to 1 based on the geometry of the propeller. It is assumed that the frame has negligible exposed area. The areas swept by the propellers while behaving as semi-permeable disks that shows resistance against the wind has a significant effect on the drag forces. The relative wind speed, $\mathbf{w}$ at the body-fixed frame of the quadcopter can be calculated as shown in equation (6).

$$\mathbf{w} = \mathbf{R}_o^e \mathbf{v}_{wind} + \mathbf{v}_{copter} \tag{6}$$

where $\mathbf{v}_{copter}$ is the quadrotor velocity, $\mathbf{v}_{wind}$ is the wind speed with respect to the earth-fixed frame, and $\mathbf{R}_o^e$ is the rotation matrix representing the mapping from earth-fixed frame to body-fixed frame. The drag force[16] experienced by the quadrotor can be represented as

$$\mathbf{f} = \frac{1}{2}\rho C_D \ \mathrm{sgn}(\mathbf{w})\mathbf{w}\mathbf{w}^{\mathrm{T}}\mathbf{a} \tag{7}$$

where C_D is the drag coefficient and is assumed to be 0.9.

Payload and battery capacity. For an aerial mapping mission, the flight time and payload capacity are crucial and the significance of having VOOPS configuration in achieving a higher payload/endurance is discussed in this section. The flight time of a quadrotor system is dependent on the payload and the battery capacity. This is because the collective upward thrust of the system will increase to maintain flight and hence the power consumption increases. As the available energy of the system is limited by the battery capacity E, the system can only sustain flight for a shorter duration. Therefore as the payload increases the flight time decreases. The battery mass m_b proportionally increases with increase in the battery capacity E and can be given by $m_b = \alpha E$, where α is battery constant which can be calculated based on the type of the battery and the configuration of the cells. Increasing the battery capacity will not increase the flight time in a linear manner due to the increase in the total weight of the system. An optimal value of the battery capacity can be found for maximum flight time for a particular payload.

The flight time is calculated by $t = E\eta/P$ as shown in equation (8) where η is the propulsion efficiency of battery, motor, and propeller combination. P is the power consumed by the system.[14,17]

$$t = \frac{4C_t^{\frac{3}{2}}}{C_q}\sqrt{\rho A} \times \left(\frac{E\eta}{((m_b + m_0 + m_p)g + 4T_{lmax})^{\frac{3}{2}} + ((m_b + m_0 + m_p)g)^{\frac{3}{2}}}\right) \tag{8}$$

where m_0 is the mass of frame, m_p is the payload mass and T_{lmax} is the maximum loss which can occur in the system due to the overlapped configuration ($T_{lmax} = 0$, for a conventional quadrotor system). The relationship between the payload, battery capacity and the flight time (endurance) for a VOOPS quadrotor is plotted in Figure 4 using equation (8) (quadrotor parameters used in the calculation are listed in Table 1).

Optimal battery capacity, $E_{Optimal}$ can be derived by maximising t with respect to E as shown in equation (9).

$$E_{Optimal} = \frac{2}{\alpha}\sqrt{\left((m_0 + m_p)^2 + \frac{(m_0 + m_p)T_{lmax}}{g} + \frac{{T_{lmax}}^2}{3g^2}\right)} \tag{9}$$

It is very important to choose the motor and propeller so as to perform flight with a total mass of $m_0 + m_p + m_{boptimal}$, where $m_{boptimal} = \alpha E_{Optimal}$. To have a quadrotor with good performance it is always better to design it in such a way that it can hover between 50 and 60% (exact value can be chosen based on the efficiency of motor propeller combination) throttle with payload. The flight time can also be improved by selecting the propulsion system with

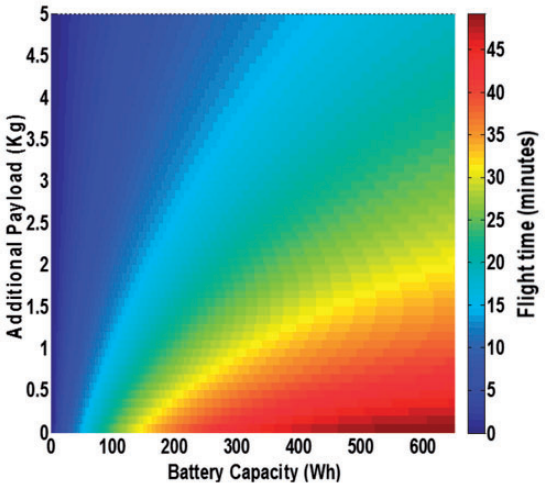

Figure 4. Battery capacity, payload and endurance.

Table 1. VOOPS quadrotor specification.

Parameters	VOOPS
Overall size (tip to tip diameter, (cm))	81.5
Battery capacity (Ah | Wh)	26 | 577.2
Coefficient of thrust, C_t	0.0121
Coefficient of propeller drag, C_q	0.0013
Blade area, A (m^2)	0.1104
Propeller radius, R(m)	0.1875
Frame mass, m_0(kg)	1.3
Payload mass, m_p(kg)	0.3
Battery mass, m_b(kg)	3.185
Overlap loss, T_{lmax} (N)	4.41
Battery constant, α	0.1225
Efficiency, η (%)	83.3

VOOPS: Vertically Offset Overlapped Propulsion System.

a better η, increased rotor disk area A, and a larger $C_t^{\frac{3}{2}}/C_q$. η and A can be increased by choosing a larger propeller. VOOPS accommodates a larger propeller for a given size and hence it has a better flight-time than the conventional systems.

Aerial mapping

To map a region, the UAV has to fly in a specific pattern and take pictures. A typical image-based aerial surveying with an UAV platform requires ground control points (GCPs) or an accurate RTK (real-time kinematic)-based GPS (global positioning system) position measurement for geo-referencing purposes. The required ground sample distance (GSD) and the on-board digital camera are to be selected based on the mission requirements. With the intrinsic parameters of the chosen camera and the GSD the mission's flying height is derived. The camera perspective centres ('waypoints') are computed based on the desired overlap of the images. Missions for detailed 3D model generation usually require high overlaps between images at low-altitude flights. The waypoints are given to the path-tracking controller which will ensure that the mission plan is executed. A stable UAV with good payload capability and endurance is required for this kind of mission. Also, the size of the UAV has to be minimal and man-packable.[18] A quadrotor vehicle is chosen here due its VTOL capabilities and the ability of the quadrotor to fly slow and closer to the ground. Being closer to ground and having a high-resolution camera will improve our GSD. VOOPS is the best option in this case as it has better endurance and payload capability when compared to the quadrotors of the same class.

Experimental VOOPS quadrotor: design specifications

VOOPS-based quadrotor system was designed to carry a camera payload and a gimbal. The total mass of the payload was estimated to be ~0.3 kg. The frame of the proposed VOOPS quadcopter was built using hollow aluminium frame as shown in Figure 5 had a mass of 1.3 kg. A 6-cell lithium polymer battery was chosen as the power source.

Using the equation (9) the battery capacity was estimated to be 25.79 Ah/572.54 Wh, which will have a mass of 3.1593 kg. The closest battery available was with a capacity of 26 Ah/577.2 Wh, which weighed 3.185 kg from *Gens Ace*™. To carry a mass of $m_b + m_0 + m_p$ and hover at 50% throttle, 15 inch propeller was the best suited.

A 400 K_v (K_v-Speed constant) BLDC motor (MN4014) from *T-motor*™ was chosen with the help of the *xcoptercalc*™ (a software to find the efficiency of a motor-propeller combination). The combined motor-propeller efficiency was calculated to be 83.3% and measured to be ~81.6%. Based on the maximum current consumption of the motor at peak r/min, electronic speed controller were chosen. Expected flight time with the current setup can be computed from the equation (8) and it was found to be approximately 45 min.

Controller design

The VOOPS quadrotor for the mapping mission requires a controller for stabilization and path tracking. A cascaded control approach is chosen here, where the path tracker, which contains a path generator, a course correction, and a position controller, feeds the set points to the attitude controller. Figure 6 shows the overall controller architecture.

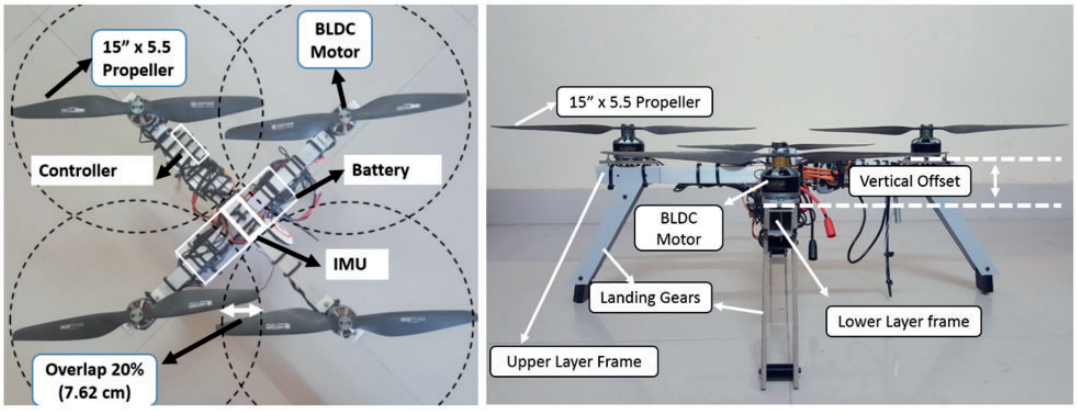

Figure 5. VOOPS, experimental vehicle.

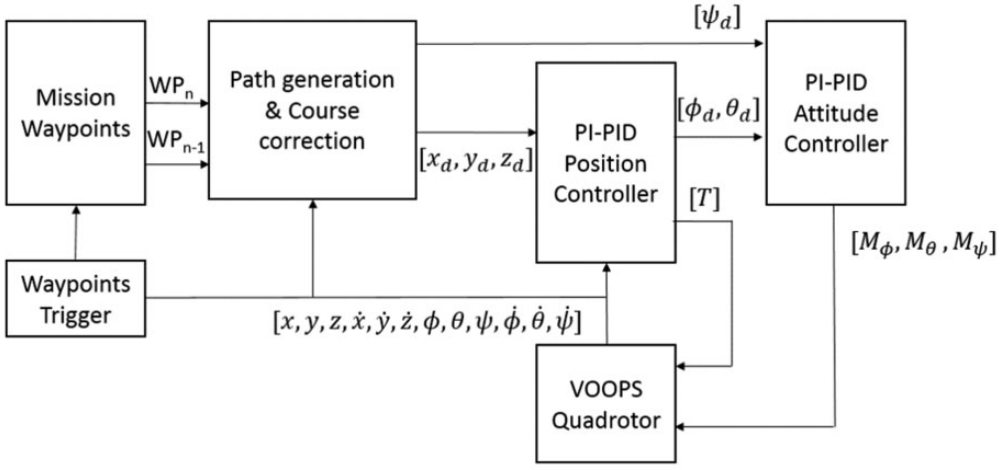

Figure 6. Path tracker control architecture.

The position/attitude controller is a cascaded PI-PID controller.[19] The inner PID loop is a velocity loop which resists the change in linear/angular velocities. This is achieved by comparing the desired rate of linear velocities/angular rotation with the GPS/gyroscope data. This makes the quadrotor stiff and reluctant to change in position/attitude. The outer PI loop controls the linear/angular position of the quadrotor which helps it position-hold/stabilize and compensates the drift in the inner loop due to the sensor noise and other disturbances. The implementation of the PI-PID controller for position and attitude are similar except the fact that the rotation matrix,[20] $\mathbf{R}_o^e$ won't appear in attitude controller.[9] The block diagram for the position controller is shown in Figure 7. Setting the right amount of gains for controller are critical to achieve stability.

The gains were tuned for the inner loop first, followed by the outer loops. Ziegler–Nichols method[21] was used to tune the gains. The same gains were used in the experimental vehicle.

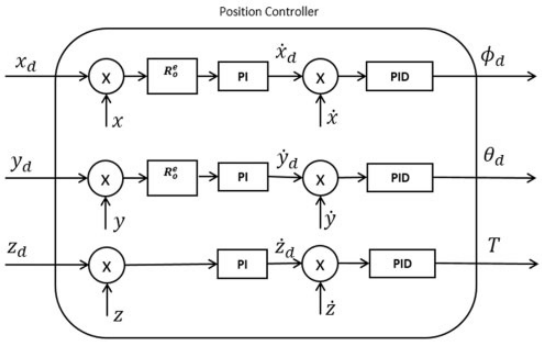

Figure 7. Position controller – Block diagram.

During the aerial mapping mission, it is important to maintain the path points in order to capture camera images at all the camera trigger points. To correct any deviation of the quadrotor from the desired path, a course correction algorithm has been implemented

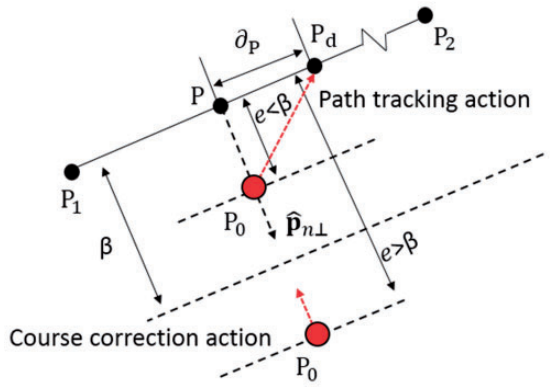

Figure 8. Path tracking and course correction illustration.

that directs the quadrotor back to the commanded path.[22]

The algorithm can be explained with the help of Figure 8. $\mathbf{p}_i$ is the position vector of the points P_i with regard to the earth-fixed frame. In the path tracker, the desired position, $\mathbf{p}_d$, can be calculated as, $\mathbf{p}_d = \mathbf{p}_o + e\hat{\mathbf{p}}_{n\perp} + \partial_P(\boldsymbol{p}_2 - \boldsymbol{p}_1/|\boldsymbol{p}_2 - \boldsymbol{p}_1|)$ where, $\mathbf{p}_o$ is the present position of the quadrotor, $\mathbf{p}$ is the projection of $\mathbf{p}_o$ on line joining P_1 and P_2 and ∂_P, is the incremental step. When the quadrotor deviates from the path, path error, e, can be calculated as, $e = (\mathbf{p}_1 - \mathbf{p}_2).(\hat{\mathbf{p}}_{n\perp})$. Here, $\hat{\mathbf{p}}_{n\perp}$ is the unit normal vector to the path. The course correction module continuously tracks e and if it is greater than a threshold, β, the desired position is set as $\mathbf{p}_d = \mathbf{p}$ so that the quadrotor corrects the cross axis error first and then moves towards the target waypoint. Figure 8 shows both the path-tracking action when $e < \beta$ and $e > \beta$.

Mission planner

Mission Planner is a Graphical User Interface (GUI) developed to help the user choose the area to be mapped. The path-tracking controller requires the waypoints as input and it is impossible for the user to specify all the waypoints for a lawn-mower pattern. The authors have developed a GUI where the user can select an area of interest by specifying the vertices of a polygon. The mission planner takes into account the flight height, overlap, and the camera parameters to provide the waypoints for the lawn mower pattern. It is also equipped to take the direction of wind into consideration to modify the pattern such that the effect of the wind does not hinder the aerial survey process. Mission planner GUI is briefly explained in this section.

The map of the required area is taken in as a georeferenced image into *MATLAB*™ using *Google maps API*™. The image obtained is centred about the home coordinates $\{x_a, y_a\}$ with the appropriate zoom from where the quadrotor will take off and land. Although the final values are going to be in latitude–longitude, the image axes are converted from latitude–longitude to distances in metres to help the user to better understand the distance between the points during mission planning. The user, using the mouse as an interface, can select points on the map. The region within the polygon formed by the points is the area to be mapped. Here, the coordinates of the vertices of the polygon are stored. The area inside the polygon has to be scanned in an organised manner (lawn mower pattern) so as to cover the entire area as shown in Figure 9. The quadrotor only slows down or speeds up when flown upwind or downwind respectively which is not a serious problem during mapping in terms of coverage. However, if there is a cross wind, the quadrotor might have difficulty staying in the planned path and might cause irregularities and serious errors during image stitching. Therefore, a prior knowledge of the wind direction would greatly help. The longest scan lines can be planned in such a way that the quadrotor need not experience cross wind which would significantly reduce such deflections. This is because the wind blowing along the direction of motion will be compensated for by the velocity controller and does not cause any deviation from the path. The wind direction is measured by the user and specified to the planner.

To align the scan lines along the wind direction (shown by dark arrow), the home coordinate frame placed at waypoint 0 (WP0) needs to be rotated about its origin as shown in step 2 in Figure 9. Then the distances between the scan lines is constructed based on the requirements of the mission such as the height, the required overlap of images, and the resolution of the images. The generated scan lines are straight lines between two waypoints and are lawn-mower like pattern and alternates between the sides of the polygon along the wind direction as shown in step 3 in Figure 9. At each intersection with the polygon, the points are recorded (waypoints 0-8). However, the waypoints are required for the original polygon. The home coordinate frame is rotated back (to the initial orientation) as shown in step 4 in Figure 9, and the final waypoints (shown in square boxes) are for tracking the area. Given the percentage of image overlap needed, the height at which quadrotor is flown, and the camera parameters, the distance between subsequent parallel paths can be found out using equation (10)

$$r_I = h\frac{S_w}{f}\frac{(1 - O_I)}{100} \tag{10}$$

where r_I is the distance between two parallel paths, f is the focal length of the camera, h is the height of flight,

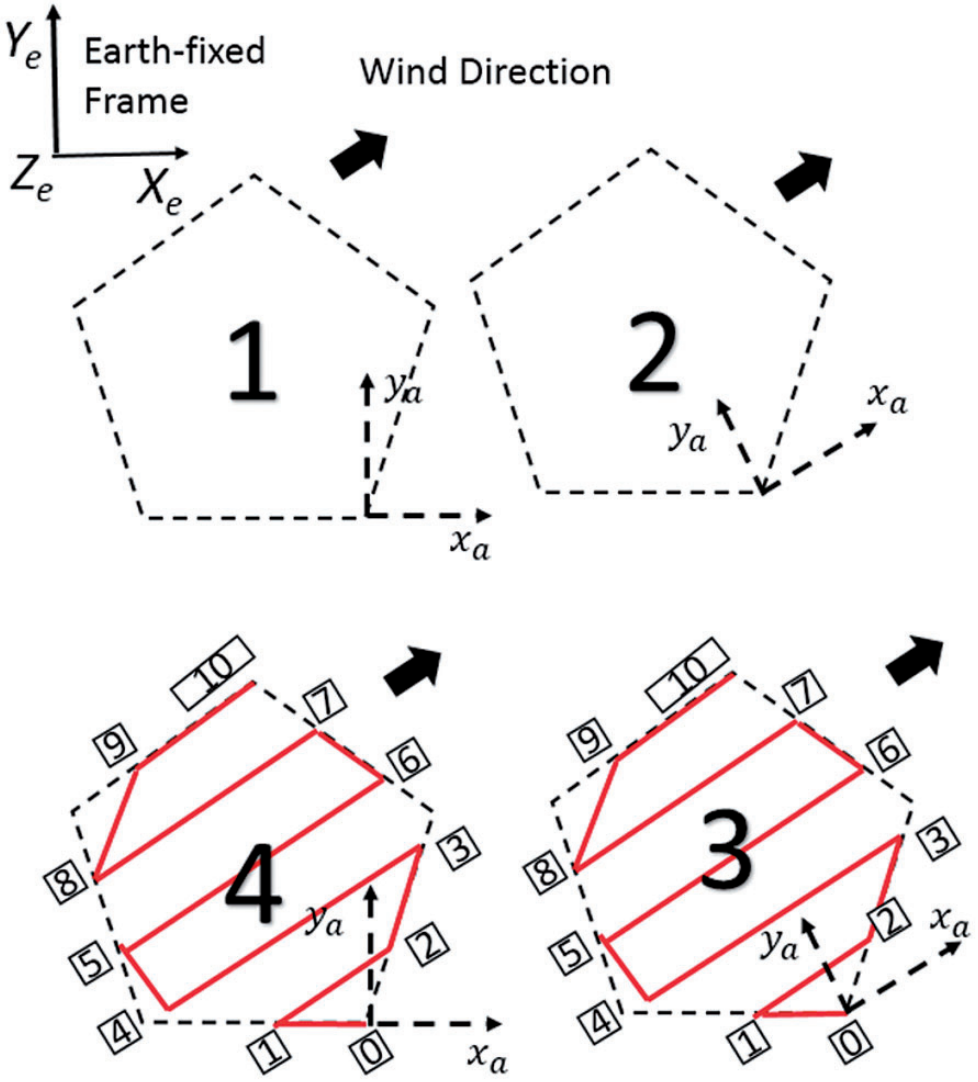

Figure 9. Area of interest polygon.

O_I is the percentage of overlap between the images and S_w represent the size of the camera sensor.

Simulation studies

Numerical simulations were performed using the mathematical model to compare the behaviour of the VOOPS quadrotor with the conventional quadrotor[11] in aerial mapping applications, as well as to check the performance of the controllers. Simulations were carried out using *MATLAB – Simulink*™. To keep the comparison fair the battery used, frame weight and the motor were the same in both the quadrotors.[11]

Attitude control

In order to simulate the performance of the attitude controller in maintaining the desired attitudes of the quadrotor, a series of inputs on pitch axis, as explained below, were given to change the pitch of quadrotor.

1. A sinusoidal variation of pitch with peak to peak of 45°.
2. A pulse of 22.5° and 45° for a duration of 4 s each.
3. An impulse at time t = 25 s.

The results of the simulation for VOOPS and a conventional quadrotor (same overall size as VOOPS, with non-overlapping propellers) are shown in Figure 10.

It is found that both the quadrotors were able to follow the sinusoidal and pulse inputs with a slight lag due to the system inertia. The impulse signals are generally difficult to be tracked and can be used to predict the responsiveness of the system. From Figure 10, VOOPS seems to have a better performance

than conventional quadrotor owing to its faster response to commanded inputs. Better response is also seen in the case of step inputs where the VOOPS is able to achieve the set point earlier than conventional quadrotor. Although the rotor inertia of VOOPS is expected to be slightly higher due to the larger propeller, it is able to better track the input signal. This is due to the force benefits of a larger propeller, which is significant than the rotor inertia differences of the propellers.

Position control

Position control performance was simulated for position hold as shown in Figure 11. Both the quadrotors were able to hold the position with minimal errors as shown in the results in Figure 12(a). In order to study the effect of wind on position hold, a uniform wind velocity of 15 m/s, 45° about Z_e was introduced at 5th second of the simulation. This is considered a strong wind for this class of quadrotors. It was found from the results that VOOPS had a slight advantage during windy condition. The response of VOOPS to wind disturbance was much faster than a conventional quadrotor due to the reasons discussed in the previous section. The quadrotors have to pitch/roll into the direction of the wind to produce forces so that it will not drift along the wind. In this process, the quadrotors expose large surface area into the wind and hence the forces generated due to the wind increases. These forces balance out with the forces generated by leaning into the wind. The quadrotor remains in the optimal roll/pitch of approximately 5° so as to balance out the wind as shown in Figure 11(b). It is also seen that a conventional copter overshoots a bit more than the VOOPS when trying to return back to the set point and this is due to the weaker propulsion system. There is a steady state error noticed during strong wind and it is due the reason that the gains were tuned for no wind condition.

The error graphs in Figure 12(a) show that the maximum error made by the conventional quadrotor happened on the onset of wind which was sudden at 5th second. The VOOPS, being a more capable copter due to its 15 inch propeller system, was able to handle the sudden wind with very minimal deviation as compared to the conventional quadrotor. The overall error characteristics show that the VOOPS is definitely having an advantage over a conventional quadrotor. The major effect is seen in the power consumed, as shown in Figure 12(b), where the conventional quadrotor

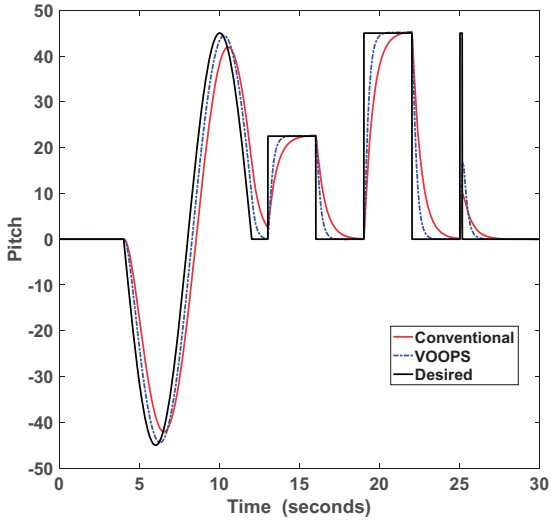

Figure 10. Simulated response for the given inputs.

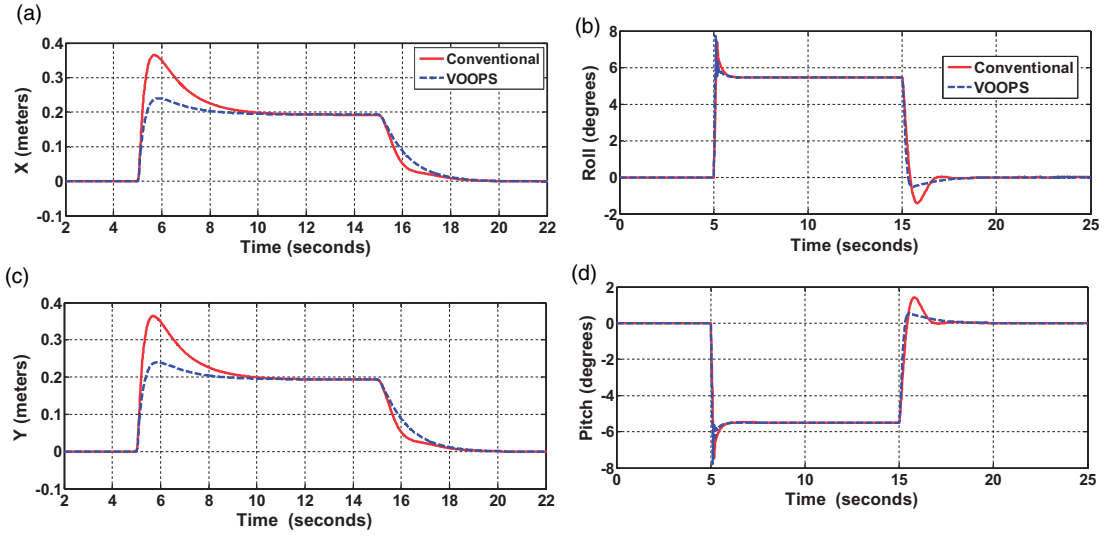

Figure 11. Simulated response for wind disturbance. (a) Position; (b) Attitude.

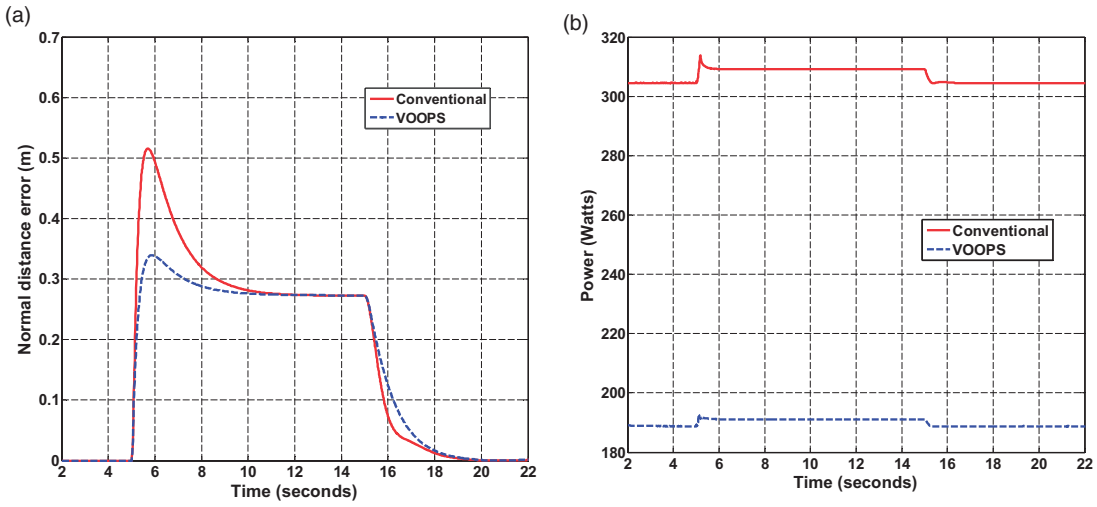

Figure 12. Normal distance error and power consumed. (a) Normal distance error; (b) Power consumed.

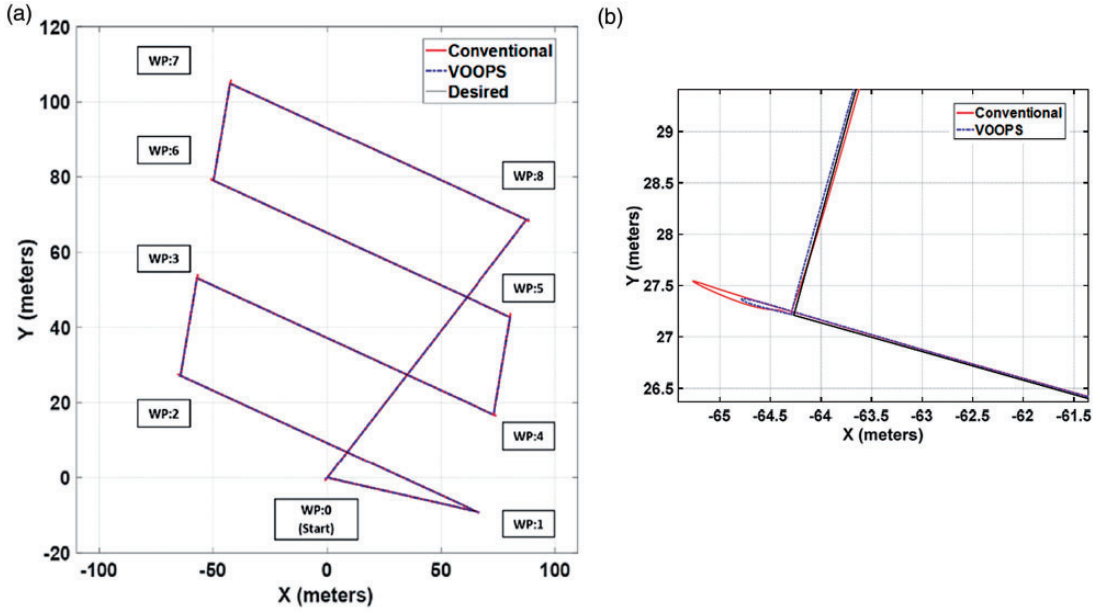

Figure 13. Simulated path: conventional vs. VOOPS. (a) Tracked path; (b) Close-up view of tracked path at WP:2.

consumes almost 68% more power than the power consumed by the VOOPS quadrotor.[11]

This is due to the reason that the conventional quadrotor operates at a very high rotor speed to maintain altitude whereas the VOOPS can produce the same force more efficiently at lower rotor speeds due to the benefits of larger propeller.

Path-tracking control

Dynamic simulation of VOOPS quadrotor and a same-size conventional quadrotor was carried out using the waypoints as shown in Figure 13(a). Waypoint 0 was set as the home point from where the launching and landing were implemented. There were eight waypoints and between two waypoints straight line path was implemented in the controller. The yaw angle was maintained towards the next waypoint throughout the mission and the coordinate frame was centred on the first waypoint.

Figure 13 shows the simulated path of the quadrotor. It is seen that the VOOPS quadrotor is able to track the path better and with lesser over shoot than conventional quadrotor. The error shown in Figure 14(a) is the

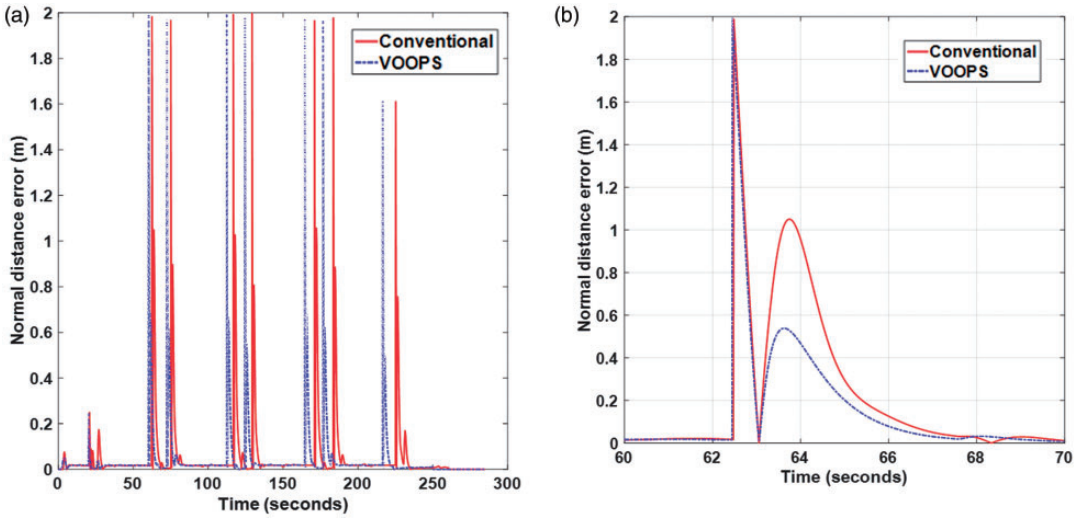

Figure 14. Tracked path errors conventional vs. VOOPS. (a) Error for full mission; (b) Error at waypoint no. 2.

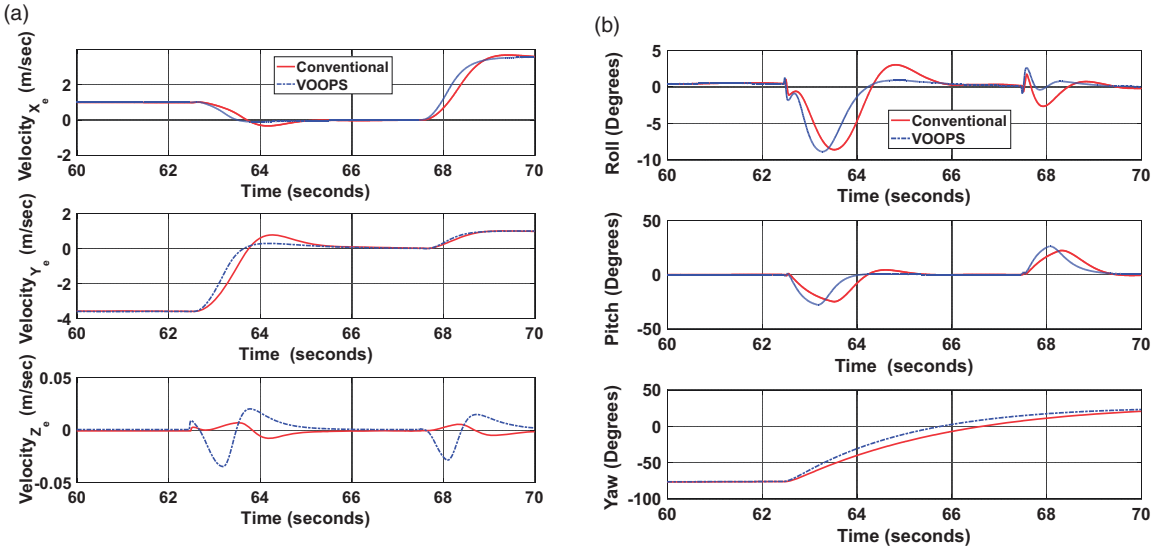

Figure 15. Linear velocities and the attitude at waypoint no. 2. (a) Linear velocities; (b) Attitude.

normal distance error between the desired and actual point for the complete mission. In both conventional and VOOPS quadrotor, the error seems to peak during the turn. This is due to the reason that the quadrotor has to stop from a forward velocity then take a turn. In Figure 14(b), the error at waypoint 2 is shown in detail. The error at sharp turns as well as the overall tracking error are high for the conventional quadrotor. In all the simulations, the controller gains were tuned using the optimizer available in $MATLAB^{TM}$.

The simulation results shown above confirm that VOOPS quadrotor was able to respond faster compared to the conventional quadrotor. This can also be seen from Figure 15 which shows the linear and angular velocity variations of both the quadrotors at waypoint 2. It is seen that both the quadrotors were travelling towards the waypoint till 63rd second and the quadrotor tried to decelerate by pitching near waypoint 2 as shown in Figure 15(b). The way in which the forward velocities are modulated, the overshoots, and the response of the VOOPS quadrotor are better than the conventional quadrotor.

The efforts involved in stopping at the waypoint, changing the heading, waiting for a specified time, and then accelerating forward towards next waypoint are shown in Figure 16. The VOOPS quadrotor is quick in generating the required moments and forces. Due to this, the overshoots are minimal and better

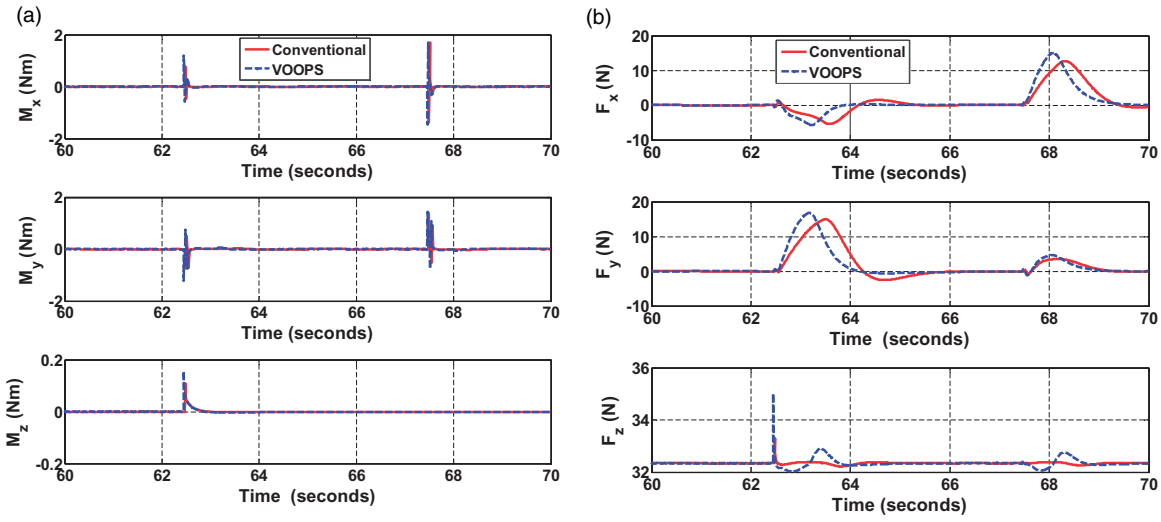

Figure 16. Forces and moments at waypoint no. 2. (a) Moments; (b) Forces.

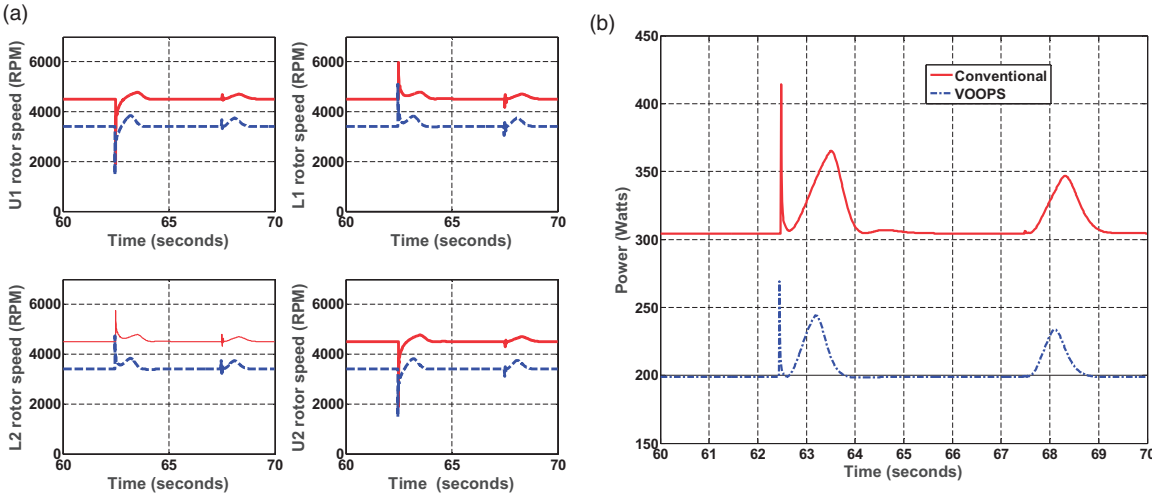

Figure 17. Rotor r/min and power consumption at waypoint no. 2. (a) Rotor speeds; (b) Power consumption.

tracking is noticed as seen in Figures 13 and 14. The Force F_z is seen during pitching or rolling to compensate for the collective thrust loss due to the tilting. The propellers spin-up rotors to maintain the altitude as shown in Figure 17(a).

The power consumed by both the quadrotors are shown in Figure 17(b). The conventional quadrotor consumes more power due to the demerits of smaller size of the propeller. The propellers in the conventional quadrotor spins almost 1500 r/min faster than the VOOPS quadrotor to produce the same amount of thrust as shown in Figure 17(a). It can be also inferred from the graphs that the corners are the most power demanding portions of the path.

One of the drawbacks of VOOPS is the loss of thrust due to overlap. Figure 18 shows the losses incurred during the mission for VOOPS system with the specifications discussed in given in Table 1. The figure shows that the loss at waypoints is on an average 3% and the maximum loss of 7.5% occur during the take-off. It is also noticed that during hover the loss is around 2.5% and the loss at the waypoints are slightly higher due to pitching/rolling, where the altitude controller spins up the rotor's to maintain height during pitch/roll and this increases the loss as shown in Figure 3.

Aerial mapping: Experiments with VOOPS quadrotor

The VOOPS quadrotor shown in Figure 5 was used for the aerial mapping experiment. A playground was chosen as the area to be mapped. Figure 19 shows

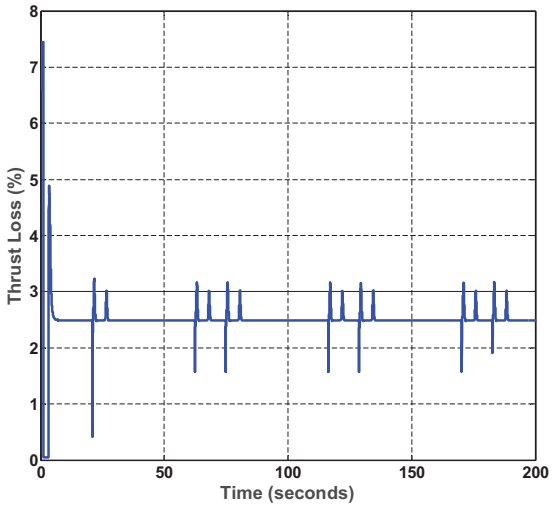

Figure 18. Loss due to the overlapped propellers.

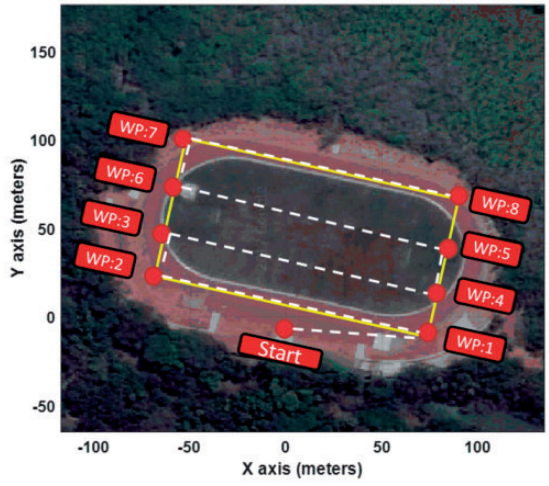

Figure 19. Planned path for aerial experiment.

the area being mapped and the path generated using the GUI. The starting point, way points and the coordinates are marked in the figure. Experimental results are discussed in the following sections.

The distance between the tracks, r_I as calculated by the mission planner was 23.4 m for a flight altitude of 15 m with a *Gopro Hero4 Black camera*. The VOOPS quadrotor during flight is shown in Figure 20.

Path-tracking experiment

Experimental VOOPS quadrotor was made to track the path and the tracking results are shown in Figure 21. A path error threshold, β, of 2 m was set during the experiment. The deviation from the planned path is shown in Figure 21(b).

The experimental deviations are mainly due to the sensor noise, wind disturbance and the GPS

Figure 20. VOOPS quadrotor in flight.

inaccuracies which were not considered during the simulations. It was found that the quadrotor was capable of tracking the planned path and the maximum tracking error was found that the quadrotor was able to operate within the allowed tolerance.

Aerial survey results

The aerial mapping was carried out using a camera having horizontal and vertical field of view as 94.4° and 122.6° respectively. The shutter speed, ISO, and aperture was set on automatic mode during the course of the mission. However, if the images have too much blur or noise, the parameters need to be manually tuned and set accordingly. For obtaining high-quality results, the maximum overlap of images is required. The desired overlap between the images was given as 35% and the desired GSD was 2 cm/pixel. For the given inputs, the desired height for the mission (15 m) was calculated, based on the camera parameters, using the equation: $h = (I_w \times GSD \times f)/(S_w \times 100)$ where I_w is the image width. Given the overlap percentage, the time interval at which the camera should trigger can be calculated. This requires the user to specify the average velocity of the copter during the course of the mission. The time elapsed between two successive images can be calculated as follows: $t = (I_h \times GSD)(1 - O_I)/100v$ where I_h is the image height and O_I is the percentage of vertical overlap and v is the average velocity the quadrotor. Using this as the time to activate the camera in time lapse mode, we get a total of 212 images during the course of the mission (Figure 23(a) shows some of these camera centres). Once the images were obtained as seen in Figure 22, the images are sorted and stitched together. In order to develop a scaled and well-oriented model

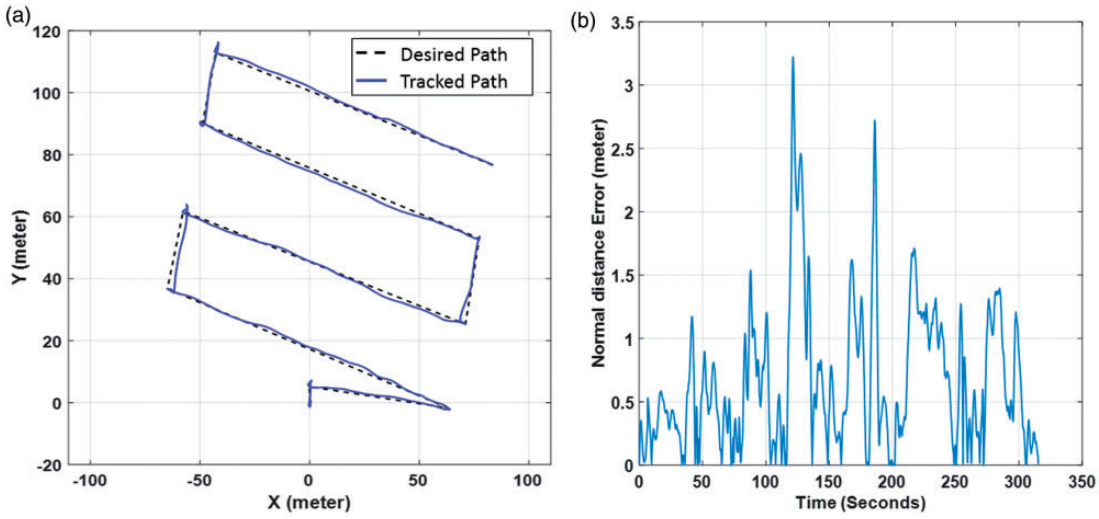

Figure 21. Experimental results. (a) Tracked position of experimental; (b) Deviation from the track.

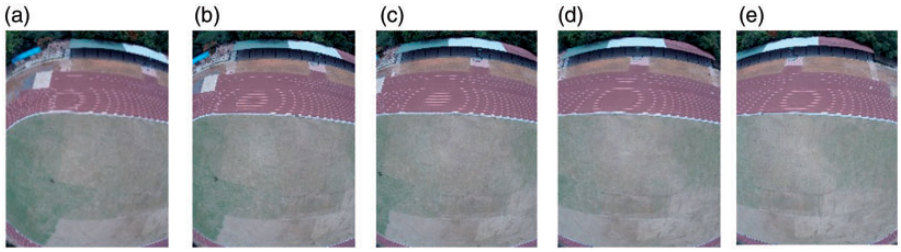

Figure 22. Sample images taken by the quadrotor.

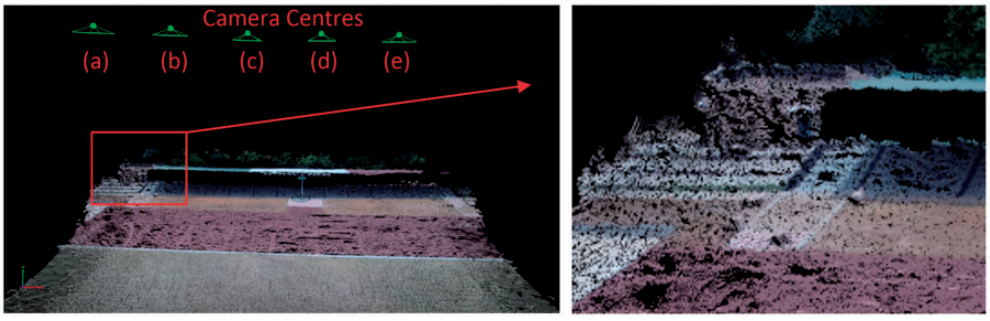

Figure 23. Point cloud data.

(geo-referenced model), it is required to know the position of the camera when the images were taken.

This information can be obtained either through geo-'location using a GPS logger directly or indirectly by providing GCPs. If neither of the information is provided, the model obtained will have no scale, orientation, and absolute position information. As a result, no metric information of the terrain can be retrieved such as the area of a particular patch of the terrain, volumetric information or distance measurements. Here GCPs were used for geo-referencing. Figure 22 shows few images and Figures 23 and 24 show the processed results, as an example. The camera centres are first estimated (shown as camera field of view and position) and the point cloud (collection of 3D points) is generated by the software using key point observations/features from overlapping images shown in Figure 23.

Inadequate overlap of images may lead to *holes* in the point cloud and therefore a lesser number of 2D

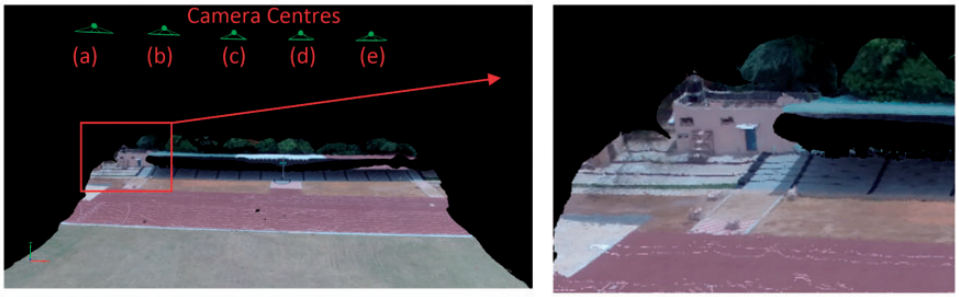

Figure 24. Meshed model.

Figure 25. Stitched ortho-rectified image.

key point observations. To overcome this, the entire point cloud is meshed as tiny triangles to fill the spaces. The image data is overlaid on top of the meshes to make the scene look close to real as seen in Figure 24. The entire model is ortho-rectified and the orthomosaic is shown in Figure 25.

Conclusion

This paper presented a novel quadrotor design and its usefulness in aerial mapping missions. Improved dynamic performance and better endurance are the two main advantages of using VOOPS in aerial missions. Payload and endurance advantages of VOOPS were discussed and compared with the conventional quadrotor of the same class and VOOPS was found to be advantageous in all aspects. Also, the choice of the battery for best flight times was discussed. The position and attitude controllers used for this purpose were discussed and tested with the dynamic model of VOOPS and also compared with conventional quadrotor. A path tracker has been developed which consists of a path generator and course correction. VOOPS and conventional quadrotor were studied during position hold with wind disturbances. A simple user interface was developed for scanning the area of interest. Simulations were carried out to analyse and compare the performance of VOOPS quadrotor with conventional in an aerial survey mission. Path-tracking experiment was conducted with the VOOPS vehicle. The path-tracking results and the aerial survey results are discussed. VOOPS has shown superior performance and best suitable for aerial survey applications.

Declaration of conflicting interests

The author(s) declared no potential conflicts of interest with respect to the research, authorship, and/or publication of this article.

Funding

The author(s) received no financial support for the research, authorship, and/or publication of this article.

References

1. Colomina I, Blázquez M, Molina P, et al. Towards a new paradigm for high-resolution low-cost photogrammetry and remote sensing. In: *International archives of photogrammetry, remote sensing and spatial information sciences*, XXI ISPRS Congress, Beijing, China, 2008, pp. 1201–1206.
2. Eisenbeiss H. *UAV photogrammetry*. PhD Thesis, ETH Zurich, Switzerland, 2009.
3. Vallet J, Panissod F, Strecha C, et al. Photogrammetric performance of an ultra-light weight Swinglet UAV. In: *International archives of photogrammetry, remote sensing and spatial information sciences,* Zurich, Switzerland, 2011, XXXVIII-1/C22, pp. 253–258.
4. Pounds P, Mahony R and Gresham J. Towards dynamically-favourable quad-rotor aerial robots. In: *Australian conference on robotics and automation*, 2004, Australian Robotics & Automation Association, Australian National University Canberra.
5. Idea Forge, Drone manufacturer and supplier, http://www.ideaforge.co.in/ (2016).
6. Verbeke J, Hulens D, Ramon H, et al. The design and construction of a high endurance hexacopter suited for narrow corridors. In: *International conference on unmanned aircraft systems (ICUAS)*, Orlando, FL, 2014, pp. 543–551. New York: IEEE.

7. Driessens S and Pounds P. The triangular quadrotor: a more efficient quadrotor configuration. *IEEE Trans Robot* 2015; 31: 1517–1526.
8. Abdilla A, Richards A, et al. Endurance optimisation of battery powered rotorcraft. In: Dixon C (ed) *Springer conference on towards autonomous robotic systems*, Liverpool, UK, 8–10 September 2015. New York: Springer International Publishing, pp. 1–12.
9. Nandakumar G, Ranganathan T, Arjun BJ, et al. Design and analysis of a novel quadrotor system VOOPS. In: *IEEE international conference on robotics and automation (ICRA)*, Seattle, USA, 26–30 May 2015, pp. 1692–1697. New York: IEEE.
10. Apostolo G. *The illustrated encyclopedia of helicopters*. New York: Bonanza Books, 1984.
11. Nandakumar G, Srinivasan A and Thondiyath A. Theoretical and experimental investigations on the effect of overlap and offset on the design of a novel quadrotor configuration, VOOPS. *J Intell Robot Sys* 2017; 92: 615–628.
12. Mullhaupt P. *Analysis and control of under-actuated mechanical non-minimum phase systems*. PhD Thesis, EPFL, 1999.
13. Stepniewski WZ and Keys CN. *Rotary-wing*. New York: Dover Publications, 1984.
14. Leishman GJ. *Principles of helicopter aerodynamics*. Cambridge: Cambridge University Press, 2002.
15. Prior SD. Reviewing and investigating the use of co-axial rotor systems in small UAVs. *Int J Micro Air Veh* 2010; 2:1–6.
16. Marino M, Fisher A, Clothier R, et al. An evaluation of multi-rotor unmanned aircraft as flying wind sensors. *Int J Micro Air Veh* 2015; 7: 285–299.
17. Johnson W. *Helicopter theory*. New York: Dover Publications, 1995.
18. Neitzel F and Klonowski J. Mobile 3D mapping with low-cost UAV system. In: *International archives of photogrammetry, remote sensing and spatial information sciences*, 2011, Zurich, Switzerland, 38, pp. 1–6.
19. Craig JJ. *Introduction to robotics: mechanics and control*. 3rd ed. Upper Saddle River: Prentice Hall, 2005.
20. Murray RM, Li Z and Sastry SS. *A mathematical introduction to robotic manipulation*. Boca Raton: CRC Press, 1994.
21. Ziegler JG and Nichols NB. Optimum settings for automatic controllers. *J Dyn Syst Meas Control* 1993; 115: 220–222.
22. Hoffmann G, Huang H, Waslander S, et al. Quadrotor helicopter flight dynamics and control: theory and experiment. In: *AIAA guidance, navigation and control conference and exhibit*, South Carolina, USA, 2007, p. 6461. South Carolina: AIAA.